Enhanced plasticity modelling of high-cyclic ratcheting and pore pressure accumulation in sands

H.Y. Liu & F. Zygounas
Section of Geo-Engineering, Department of Geoscience and Engineering
Delft University of Technology, Delft, The Netherlands

A. Diambra
Department of Civil Engineering, Faculty of Engineering
University of Bristol, Bristol, UK

F. Pisanò
Section of Geo-Engineering, Department of Geoscience and Engineering
Section of Offshore Engineering, Department of Hydraulic Engineering
Delft University of Technology, Delft, The Netherlands

ABSTRACT: Predicting accurately the response of sands to cyclic loads is as relevant as still challenging when many loading cycles are involved, for instance, in relation to offshore or railway geo-engineering applications. Despite the remarkable achievements in the field of soil constitutive modelling, most existing models do not yet capture satisfactorily strain accumulation under high-cyclic drained loading, nor the the build-up of pore pressures under high-cyclic undrained conditions. Recently, bounding surface plasticity enhanced with the concept of memory surface has proven promising to improve sand ratcheting simulations under drained loading conditions (Corti et al. 2016). This paper presents a new model built by combining the memory surface concept by Corti et al. (2016) with the well-known SANISAND04 bounding surface formulation proposed by Dafalias and Manzari (2004). The outcome is a new sand model that can reproduce phenomenologically the fabric evolution mechanisms governing strain accumulation under long-lasting loading histories (here up to 10^4 loading cycles). In undrained test simulations, the model proves capable of correctly capturing the rate of pore pressure accumulation, preventing precocious occurrence of cyclic liquefaction.

1 INTRODUCTION

Predicting accurately the response of sands to cyclic loads is still challenging when many loading cycles are involved. More specifically, cyclic accumulation of permanent strain and pore water pressure may lead to reduction of capacity, serviceability and fatigue resistance (Andersen 2015). The term 'ratcheting' is adopted to denote the gradual accumulation of plastic strains under loading cycles (Houlsby et al. 2017). In engineering practice, soil ratcheting is often described by using empirical equations derived from experimental measurements (Pasten et al. 2013). Empirical formulations of this kind may be found for long-term strain accumulation phenomena (Sweere 1990, Lekarp and Dawson 1998, Wichtmann 2005) and short-term pore pressure build-up during earthquakes or storms (Seed et al. 1975, Green et al. 2000, Idriss and Boulanger 2006). Although empirical equations have proven efficient to use, some limitations stand out clearly: (1) high-cyclic tests for calibrating empirical relations are usually costly and time-consuming; (2) the use of reconstituted sand specimens goes beyond the scope of standard soil characterisation. An alternative approach is to set up a reliable advanced constitutive model that can capture satisfactorily sand ratcheting and related strain/pore-water-pressure accumulation trends under different cyclic loading conditions and drainage scenarios.

In this work, the memory surface concept is combined with the structure of the model prosed by Dafalias & Manzari (2004) (SANISAND04 model). The reference SANISAND04 model, which is build upon a critical state and bounding surface plasticity framework, includes a fabric-dilatancy tensor to reproduce soil fabric effects. The suitability of combining bounding surface theory and memory surface concept has been proven by the work of Corti et al.

(2016). Soil fabric and its evolution are recorded by a newly introduced memory surface, enclosing a stress region which the soil feels to have already experienced and thus characterised by high stiffness.

The main purpose of the paper is to provide a reliable constitutive model to: (1) complement/replace demanding laboratory sand testing as input to displacement/rotation accumulation procedures; (2) enhance the real time-domain simulation during shorter cyclic loading histories. The proposed model is validated by simulating results of experimental tests performed on a quartz sand and the Karlsruhe sand under cyclic loading conditions. The experimental data regard both drained (Wichtmann 2005) and undrained (Wichtmann and Triantafyllidis 2016) triaxial tests investigating the influence of varying the mean confining pressure, cyclic stress amplitude and void ratio.

2 MODEL FORMULATION

2.1 *General modelling strategy*

The proposed model improves the cyclic performance of SANISAND04 by introducing a memory surface to keep track of relevant fabric effects and to simulate realistic sand cyclic behaviour under both drained and undrained loading conditions. The selected backbone bounding surface model (SANISAND04 model) was developed by Dafalias & Manzari (2004), with a fabric-dilatancy tensor defined to take into account the effects of increased dilation following cyclic contractive behaviour. In SANISAND04, soil stiffness is determined by the distance between current stress state and its conjugate point on the bounding surface. However, the fabric-dilatancy tensor, which only activates if the stress path crosses the phase transformation line (PTL), is not sufficient to fully describe the influence of soil fabric especially when the soil is responding within its contractive regime. Therefore, SANISAND04 is less suitable for simulating soil progressive stiffening during cyclic loading, since it will overpredict strain accumulation and the rate of pore pressure build-up. The proposed model introduces a circular-shape memory surface as a third model surface in the normalised π plane, as illustrated in Figure 1. The memory surface evolves during the loading process following three main rules: (1) changes size and position with plastic strains to simulate gradual evolution of the soil fabric; (2) always encloses the current stress state and (3) always enclose the yield surface. The bounding, critical and dilatancy surfaces are defined using an Argyris-type shape to capture the response of the soil at varying load angle. The adoption of state parameter Ψ (Been and Jefferies 1985), defined as the difference between the current void ratio and the critical void ratio ($\Psi = e - e_c$) at the same mean stress level, allows to reproduce the influence of the void ratio over the whole loose-to-dense range. For the critical state line, a power relationship is adopted as suggested by (Li and Wang 1998). The complete model formulation is presented in the work of Liu et al. (2018), following the previous developments by Corti et al. (2016).

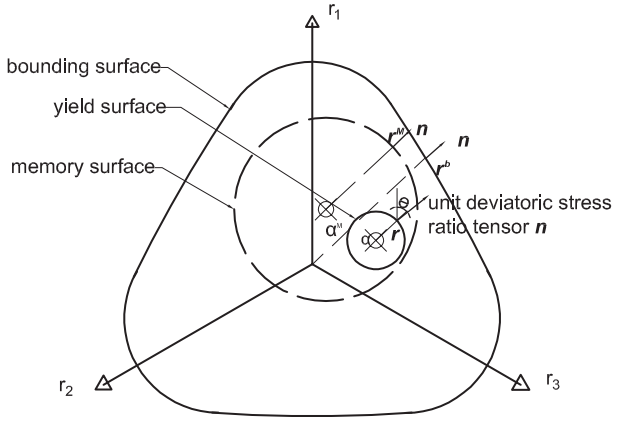

Figure 1: Visualisation in the π-plane of the three-surface model formulation

2.2 *Implementation of the memory surface*

Introduction of the memory surface is linked to a modification of the hardening coefficient h, see Equation 1:

$$h = \frac{b_0}{(\mathbf{r} - \mathbf{r}_{in}) : \mathbf{n}} \exp\left[\mu_0 \left(\frac{p}{p_{atm}}\right)^{0.5} \left(\frac{b^M}{b_{ref}}\right)^2\right] \quad (1)$$

Here, $b^M = (\mathbf{r}^M - \mathbf{r}) : \mathbf{n}$ denotes the distance between current stress ratio point $\mathbf{r}$ and its image point on memory surface $\mathbf{r}^M$, projecting along the direction of unit normal to the surface $\mathbf{n}$. The dependency of h on the current pressure p through the term $(p/p_{atm})^{0.5}$ is introduced to improve the original formulation of Corti et al. (2016) and follows some findings from Corti et al. (2017). Definitions for b_0 and $\mathbf{r}_{in}$ are the same as in Dafalias & Manzari (2004). p_{atm} is the atmospheric pressure. b_{ref}, which is adopted for normalisation, is the reference distance indicates the size of bounding locus along the current load angle. The memory-surface-related parameter μ_0 quantifies the influence of fabric effects on soil stiffness, especially in the transition from ratcheting to shakedown behaviour. In this case, soil stiffness depends not only on the relative distance between current stress state ($\mathbf{r}$) and its image point on bounding surface ($\mathbf{r}^b$), but also on the distance between $\mathbf{r}$ and its image point on memory surface ($\mathbf{r}^M$). This is reflected in the expression of the hardening modulus K_p in Equation 2.

$$K_p = \frac{2}{3} p h (\mathbf{r}^b - \mathbf{r}) : \mathbf{n} \quad (2)$$

The evolution of memory surface center $\boldsymbol{\alpha}^M$ is assumed to be along the direction $\mathbf{r}^b - \mathbf{r}^M$ - see Equation 3:

$$d\boldsymbol{\alpha}^M = \frac{2}{3} \langle L \rangle h^M (\boldsymbol{r}^b - \boldsymbol{r}^M) \quad (3)$$

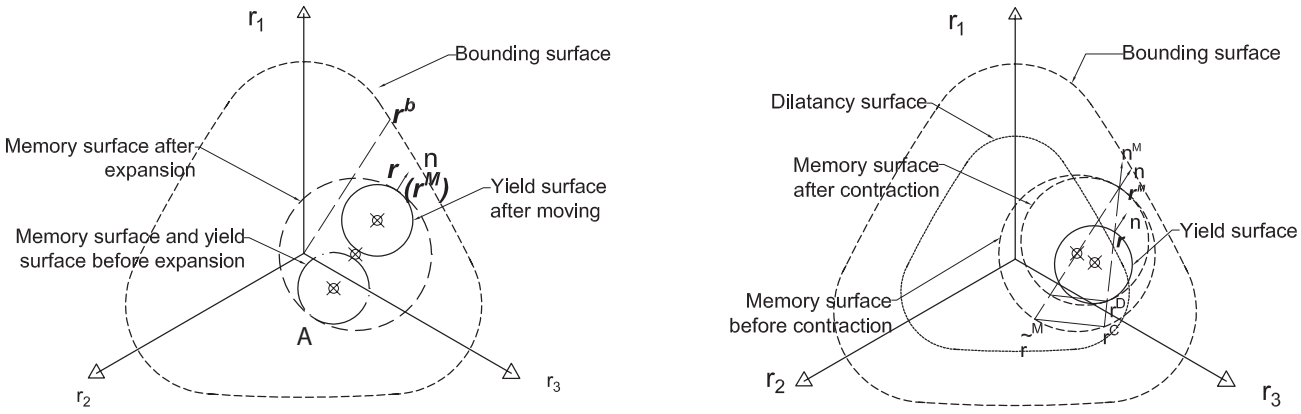

(a) memory surface expansion

(b) memory surface shrinkage

Figure 2: Evolution of the memory surface size: (a) memory surface expansion during virgin loading conditions; (b) memory surface shrinkage during dilative straining.

The evolution of memory surface size is shown mathematically with Equation 4. From experimental observations, contractive soil behaviour (positive volumetric strain by geotechnical convention) leads to more stable soil fabric configuration and therefore, stiffer soil behaviour. Thus, it is reasonable to link it with an expansion of the memory surface. The expansion of the memory surface mainly take places during virgin loading (see Figure 2(a)), which is defined as the state when the yield and memory surfaces are tangential to each other at the current stress point. The size of the memory surface is linked to the variable m^M and its expansion is linked to the evolution of memory surface center, as shown in the first term of the Equation 4 (i.e., $\sqrt{2/3}d\boldsymbol{\alpha}^M : \boldsymbol{n}$):

$$dm^M = \sqrt{\frac{3}{2}}d\boldsymbol{\alpha}^M : \boldsymbol{n} - \frac{m^M}{\zeta}\left(1 - \frac{x_1 + x_2}{x_3}\right)\langle -d\varepsilon_v^p\rangle \quad (4)$$

Here, $x_3 = (\mathbf{r}^M - \mathbf{r}^C) : \mathbf{n}^M$, $x_1 + x_2 = (\mathbf{r}^M - \mathbf{r}^D) : \mathbf{n}^M$ (see Figure 2(b)). The unit tensor $\mathbf{n}^M$ represents the direction of $\mathbf{r}^M - \mathbf{r}$. During virgin loading conditions, soil stiffness is governed only by the distance between the current stress and its image on the bounding surface. Under non-virgin conditions (for example after load reversal), the memory surface acts as an additional bounding surface. Soil stiffness is increased by the non-zero distance b^M (see Equation 1) between yield surface (f) and memory surface (f^M). Stiffer soil behaviour is captured in this manner.

By contrast, dilative soil behaviour leads to a weaker granular arrangement (also known as 'fabric damage'), and the soil loses part of its stiffness. This situation can therefore be linked to the shrinkage of the memory surface size. In the model, the memory surface contraction mechanism, or fabric damage mechanism, only activates when negative plastic volumetric strains are generated. As presented by the second term of Equation 4, if positive volumetric strains are generated, $\langle -d\boldsymbol{\varepsilon}_v^p\rangle = 0$ because of the Macauley brackets. The reduction in memory surface size, which is schematically described in Figure 2(b), happens on the opposite side of $\mathbf{r}^M$, along the direction ($\mathbf{r}^M\mathbf{r}^C$). To guarantee that the yield surface always lies inside the memory surface, the size reduction ends if the memory surface and the yield surface become tangential to each other at the contraction point (in other words, when $1 - (x_1 + x_2)/x_3 = 0$), even if the soil is still experiencing negative volumetric strain. The reduction rate of memory surface size is controlled by the parameter ζ.

2.3 *Enhanced dilatancy coefficient*

In SANISAND04, a fabric-dilatancy tensor is introduced into the flow rule, or to be more specific, into the dilatancy coefficient D. The feature is introduced to reproduce the experimental observation that when stress path crosses the PTL and load increment reversal is imposed, there is an obvious increase in pore water pressure build-up with respect to the number of cycles under undrained cyclic loading conditions. The underlying mechanism is the change of fabric orientation. Instead of using a single tensor, the proposed model accounts for fabric effects through the relative position and distance between the memory surface and the dilatancy surface, according to Equation 5:

$$D = A_d(\boldsymbol{r}^d - \boldsymbol{r}) : \boldsymbol{n} \qquad A_d = A_0 \exp\left(\beta \frac{\left\langle \tilde{b}_d^M \right\rangle}{b_{ref}}\right) \quad (5)$$

In this work, whether the sand is more prone to dilation or contraction is determined by the term $\tilde{b}_d^M = (\tilde{\mathbf{r}}^d - \tilde{\mathbf{r}}^M) : \mathbf{n}$, which basically modulates the magnitude of D (not the sign) depending on the occurrence of previous dilation or contraction. The graphical representation of this mechanism is provided in

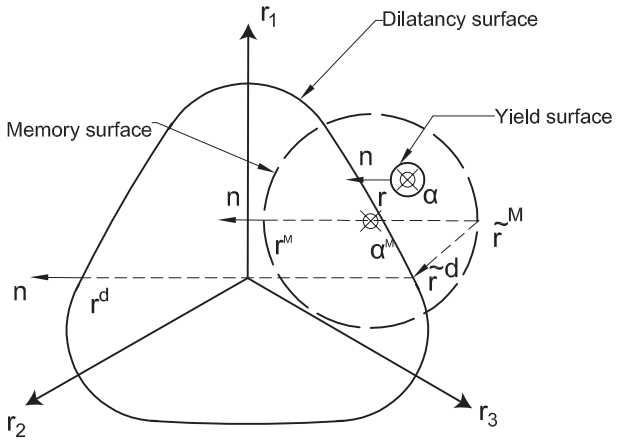

Figure 3: Illustration of image points for modifying current dilatancy coefficient.

Figure 3. If $\tilde{b}_d^M > 0$, the soil has experienced dilation during the previous loading process, implying a sort of 'contraction bias' under subsequent unloading. The dilatancy D is enlarged because of a larger dilation coefficient A_d by noticing that the term $\exp\left(\beta \left\langle \tilde{b}_d^M \right\rangle / b_{ref}\right) > 1$ in this situation. In this way, the model can simulate more significant pore water pressure build-up under undrained loading. Conversely, if $\tilde{b}_d^M < 0$, soil fabric orientation is biased toward dilation, $\exp\left(\beta \left\langle \tilde{b}_d^M \right\rangle / b_{ref}\right) = 1$. It should be noted that the dilatancy coefficient in Equation 5 substitutes the fabric-tensor concept used by Dafalias and Manzari (2004), and the two associated constitutive parameters.

3 MODEL CALIBRATION

The model parameters can be divided into two sets. The first set can be entirely derived from monotonic tests, although they influence the cyclic performance as well (from G_0 to n^d in Table 1 and Table 2). Their calibration rely on drained and/or undrained monotonic triaxial tests (Dafalias and Manzari 2004, Taiebat and Dafalias 2008). The second set contains the memory surface related parameters i.e., μ_0, ζ and β in the Table 1, which can be estimated by fitting procedures (Liu et al. 2018). Calibration of μ_0 can be more easily achieved through cyclic tests where the soil is experiencing contractive behaviour. In this condition, ζ and β, have no influence on the model prediction because of the absence of dilative soil behaviour. Conversely, calibration of ζ and β requires tests with (at least part of) loading paths crossing the PTL. In particular, the parameter β controls the reduction rate of the mean effective stress during undrained loading after stages of dilative deformation (after which more pronounced effective stress reduction is observed experimentally).

In Table 1, model parameters for a quartz sand are calibrated based on the experimental work conducted by Wichtmann (2005). Six sets of drained monotonic triaxial tests are used for calibrating the monotonic parameters, while memory surface-related parameters are calibrated based on the strain accumulation curve with loading cycles up to 10^4. Table 2 lists model parameters for the Karlsruhe fine sand-experimental data published by Wichtmann and Triantafyllidis (2016). In total, 10 sets of drained and undrained monotonic triaxial tests are simulated to identify the monotonic parameters. For the memory surface parameters, the calibration relies on isotropic cyclic triaxial undrained tests, using the observed trends of accumulated pore water pressure ratio against number of cycles.

4 MODEL VALIDATION

4.1 *Drained tests*

For the drained case, model parameters are calibrated against experimental results from Wichtmann (2005) on a quartz sand, as listed in Table 1. For memory surface-related parameters, the calibration procedure relies on the drained cyclic test with $e_{in} = 0.674$, with other load conditions the same as described in Figure 4. Performance of the proposed model is validated through the comparison between triaxial experimental results and simulation results under cyclic loading conditions, with focus on different initial void ratio and different cyclic stress amplitude q^{ampl}. Wichtmann's experiments concern one-way asymmetric cyclic loading performed in two stages: after the initial isotropic consolidation up to $p = p_{in}$, p-constant shearing is first performed to reach the target average stress ratio $\eta^{ave} = q^{ave}/p_{in}$; then, cyclic axial loading at constant radial stress is applied to obtain cyclic variations in deviatoric stress q about the average value q^{ave}, i.e. $q = q^{ave} \pm q^{ampl}$. High-cyclic sand parameters are tuned to match the evolution during regular cycles of the accumulated strain norm ε^{acc} defined through the accumulated axial strain ε_a^{acc} and accumulated radial strain ε_r^{acc}, as:

$$\varepsilon^{acc} = \sqrt{(\varepsilon_a^{acc})^2 + 2(\varepsilon_r^{acc})^2} \tag{6}$$

4.1.1 *Influence of initial void ratio*

The influence of the soil initial void ratio on soil drained cyclic behaviour is studied by performing drained triaxial tests on soil samples with initial void ratios $e_{in} = 0.803$, 0.674 and 0.580. Other loading parameters are kept unaltered: $p_{in} = 200\ kPa$, $\eta^{ave} = 0.75$ and $q^{ampl} = 60\ kPa$. Comparison between experimental results and model simulations are presented in Figure 4. Based on the experimental observations, denser sand specimens accumulate less strains. The model seems to capture quantitatively well all relevant trends. The model also accurately predicts the accumulated strain for the cases of $e_{in} = 0.803$ and 0.674, the loose and medium dense sand. However, for the dense sample $e_{in} = 0.580$, the model slightly overestimates the accumulated strain.

Table 1: Model parameters for the quartz sand for drained cyclic simulations

Elasticity		Critical state					Yield surface	Plastic modulus			Dilatancy		Memory surface		
G_0	ν	M	c	λ_c	e_0	ξ	m	h_0	c_h	n^b	A_0	n^d	μ_0	ζ	β
130	0.05	1.25	0.702	0.015	0.81	0.7	0.01	5.05	1.05	2.25	1.06	1	270	0.0005	0.2

Table 2: Model parameters for the Karlsruhe fine sand for undrained cyclic simulations

Elasticity		Critical state					Yield surface	Plastic modulus			Dilatancy		Memory surface		
G_0	ν	M	c	λ_c	e_0	ξ	m	h_0	c_h	n^b	A_0	n^d	μ_0	ζ	β
95	0.05	1.35	0.85	0.056	1.038	0.28	0.01	7.6	1.015	1.2	0.56	2.15	85	0.0001	6

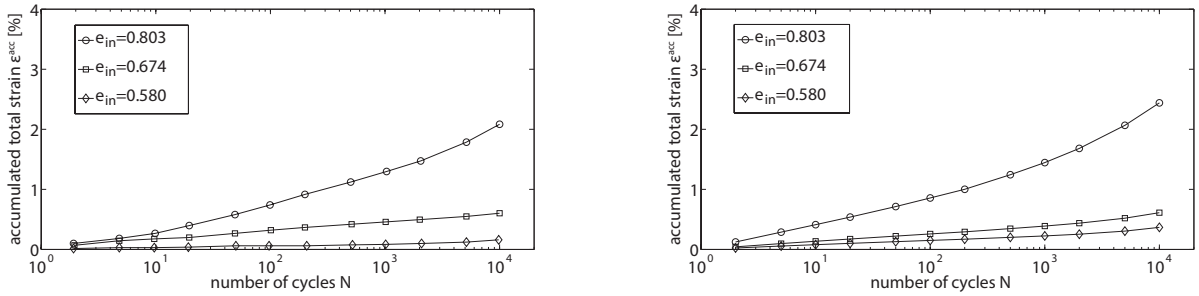

(a) Experimental results

(b) Simulation results

Figure 4: Influence of soil density on strain accumulation under drained conditions (a) experimental results; (b) simulation results. Confining pressure $p_{in} = 200\ kPa$, stress obliquity $\eta^{ave} = 0.75$, stress amplitude $q^{ampl} = 60\ kPa$.

4.1.2 *Influence of cyclic stress amplitude*

The impact of the cyclic stress amplitude on the accumulated permanent stain under drained cyclic conditions is studied by performing three different stress amplitudes ($q^{ampl} = 80\ kPa$, $60\ kPa$ and $31\ kPa$) on three soil samples. In the tests, confining pressure $p_{in} = 200\ kPa$, stress obliquity $\eta^{ave} = 0.75$, initial void ratio $e_{in} = 0.702$ are considered. Comparison between experimental results and model simulations are presented in Figure 5. The experimental results show that increasing cyclic stress amplitude leads to larger accumulated strain, corroborating findings of other experimental works (Escribano et al. 2018). This is successfully predicted by the model, see Figure 5.

4.2 *Undrained tests*

The undrained perfromance of the model is validated by comparing model simulations with five sets of experimental results by Wichtmann and Triantafyllidis (2016) on Karlsruhe fine sand. Model parameters are listed in Table 2. The results are presented in terms of accumulated pore water pressure ratio (r_u, which represents the accumulated pore water pressure u^{acc} normalised by the initial effective confining pressure, i.e. $r_u = u^{acc}/p'_{in}$). Parameters μ_0, ζ and β are calibrated by fitting the experimental data presented in Figure 6(b).

4.2.1 *Influence of initial effective confining pressure and void ratio*

In Figure 6, three sets of results are presented with simulation results from both the new model and the original SANISAND04 model. For all three sets of results, the simulation of the SANISAND04 model show clear liquefaction with accurate ultimate r_u level. However, the predicted number of cycles to liquefaction is in all instances too low. In other words, SANISAND04 underestimates significantly the resistance to liquefaction, especially as the void ratio deviates from e_{max}.

The impact of the initial void ratio is studied by combing the test results on medium dense sand (Figure 6(a), the initial void ratio $e_{in} = 0.825$) with the dense sand results (Figure 6(b), the initial void ratio $e_{in} = 0.759$). For both tests, the initial effective pressure $p'_{in} = 100\ kPa$, the cyclic stress ratio ς, defined as $\varsigma = q^{ampl}/p'_{in}$, equals to 0.3. A slower increasing of r_u is observed compared to that of for denser sand. It indicates that under the same loading condition, the resistance to liquefaction for dense sands is higher than for loose sands. The new model predicts the ultimate r_u level and number of loading cycles in a reasonable accurate magnitude with a single set of parameters, especially for the dense sand.

The influence of the initial effective confining pressure p'_{in} is shown in Figure 6(a) and Figure 6(c). For both tests, $\varsigma = 0.3$. In Figure 6(b), the initial effective confining pressure $p'_{in} = 100\ kPa$ and the number of cycles N to liquefaction is 54. For Figure 6(c), $p'_{in} = 300\ kPa$ and $N = 269$. Overall, the new model

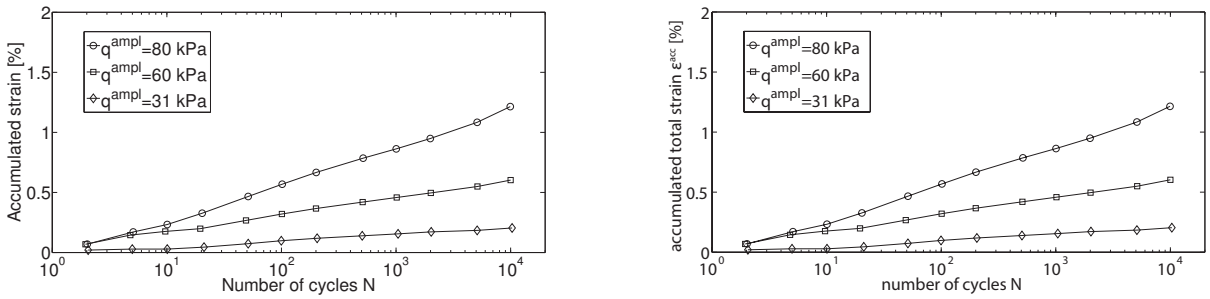

(a) Experimental results (b) Simulation results

Figure 5: Influence of cyclic stress amplitude on strain accumulation under drained conditions (a) experimental results; (b) simulation results. Confining pressure $p_{in} = 200\ kPa$, stress obliquity $\eta^{ave} = 0.75$, initial void ratio $e_{in} = 0.702$.

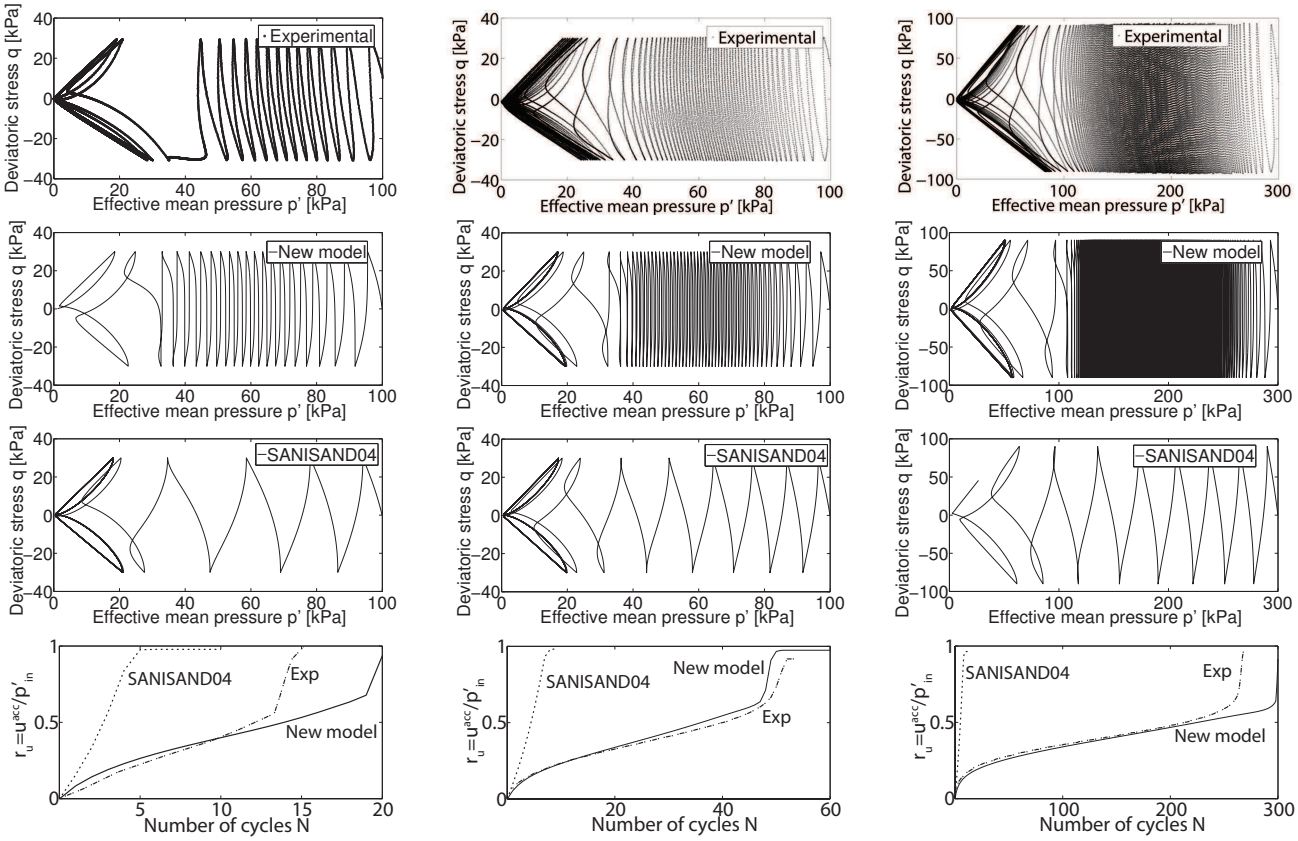

(a) $p'_{in} = 100\ kPa$, $e_{in} = 0.825$ (b) $p'_{in} = 100\ kPa$, $e_{in} = 0.759$ (c) $p'_{in} = 300\ kPa$, $e_{in} = 0.744$

Figure 6: Influence of initial effective confining pressure p'_{in} and initial void ratio e_{in} on soil undrained cyclic behaviour, with a drained cycle be applied prior to the undrained cycles. (a) $p'_{in} = 100\ kPa$, $e_{in} = 0.825$; (b) $p'_{in} = 100\ kPa$, $e_{in} = 0.759$; (c) $p'_{in} = 300\ kPa$, $e_{in} = 0.744$. All tests with $\varsigma = 0.3$.

predicts satisfactory the undrained behaviour at both qualitative and quantitative levels.

4.2.2 *Influence of cyclic stress ratio*

Cyclic triaxial tests are conducted on two soil samples at $\varsigma = 0.2$ and $\varsigma = 0.25$, respectively. For both tests, the effective confining pressure is $p'_{in} = 200\ kPa$. The results are shown in Figure 7. The experimental results in Figure 7(a) indicate that for the soil sample with $e_{in} = 0.842$ and $\varsigma = 0.2$, liquefaction occurs after 146 loading cycles. The other soil sample, with $e_{in} = 0.813$ and $\varsigma = 0.25$, undergoes 77 loading cycles before liquefaction under the same loading conditions, see Figure 7(b). It indicates that the looser sample subjected to smaller cyclic stress amplitude resists more to liquefaction compared with the denser sample under larger cyclic stress amplitude. Again, SANISAND04 predicts higher pore water pressure generation for each cycle, while the new model performs substantially better.

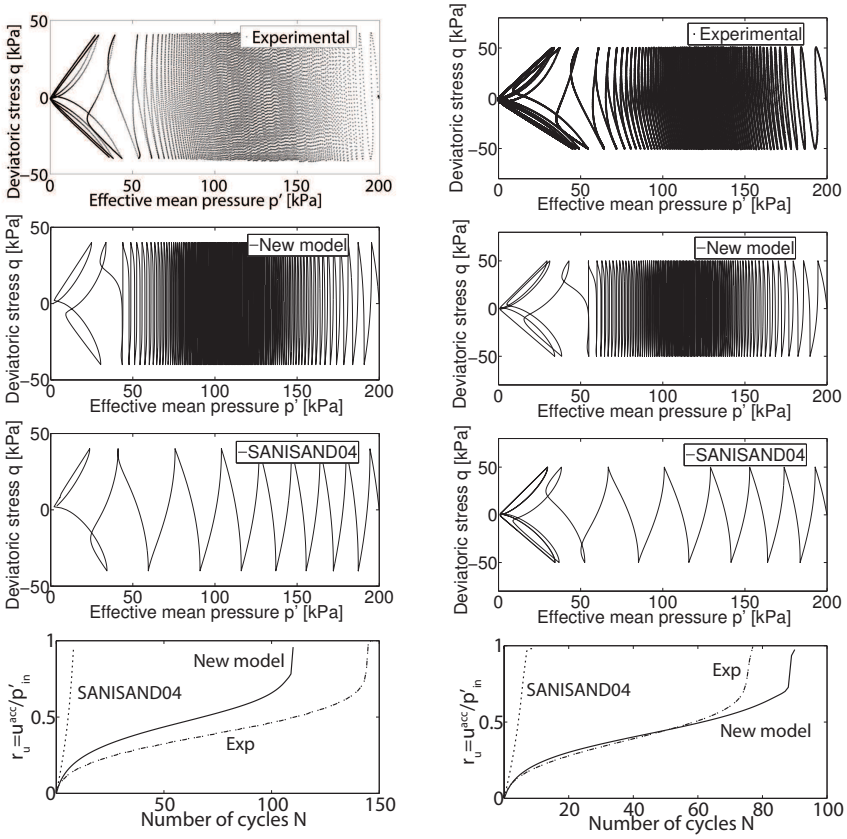

(a) $e_{in} = 0.842$, $\varsigma = 0.2$ (b) $e_{in} = 0.813$, $\varsigma = 0.25$

Figure 7: Influence of cyclic stress ratio ς on soil undrained cyclic behaviour, with a drained cycle be applied prior to the undrained cycles. Effective confining pressure $p'_{in} = 200\ kPa$, (a) $e_{in} = 0.842$, $\varsigma = 0.2$; (b) $e_{in} = 0.813$, $\varsigma = 0.25$.

4.2.3 *Best-fit simulations*

For all undrained tests above, only one single set of parameters has been adopted, including an average value of μ_0 equal to 85. The model performs well in (both qualitatively and quantitatively) capturing the undrained cyclic behaviour under different loading conditions and relative densities. This demonstrates that the strategy of combining memory surface concept with bounding surface hardening theory is suitable to analyse the influence of fabric effects in cyclic loading problems. However, better simulation results are possible if different values of memory surface parameters are adopted for different tests. In Figure 8, five different μ_0 values are adopted to simulate the aforementioned five undrained cyclic triaxial tests (Wichtmann and Triantafyllidis 2016). Simulation results are presented in terms of $u_r - N$. Simulation results with different μ_0 values fit the experimental results better than that of the simulation results obtained using $\mu_0 = 85$ for all tests. This indicates that even if the modelling strategy is suitable, better memory surface evolution law and more suitable flow rule can still be devised.

5 CONCLUSIONS

In this work, a new model was proposed by introducing the memory surface hardening theory into SANISAND04 model to properly simulate sand ratcheting and pore pressure accumulation under high-cyclic loading. The memory surface, which is allowed to evolve both in size and position in this model, represents phenomenologically the evolution of sand fabric during repeated loading. The model predictions agrees well with both drained and undrained cyclic triaxial experimental results under different loading conditions and different soil densities. The validation of the model allowed to check its accuracy with respect to the following aspects: (1) progressive soil stiffening at increasing number of cycles; (2) larger accumulated strain for looser soil samples under drained loading conditions at given cycles; (3) larger accumulated strain for larger stress amplitude under drained loading conditions at given number of cycles; (4) prediction of pore water pressure accumulation under different undrained cyclic loading conditions and soil densities. Overall, the model has promising potential to complement costly high-cyclic laboratory tests, as well as to be employed in time-domain simulations of cyclic/dynamic soil-structure interaction problems.

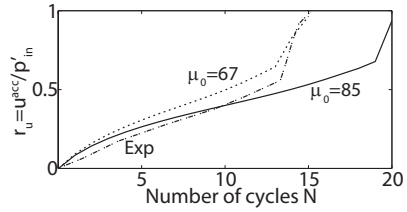

(a) test settings: $p'_{in} = 100\ kPa$, $e_{in} = 0.825$, $\varsigma = 0.3$, best fit $\mu_0 = 67$

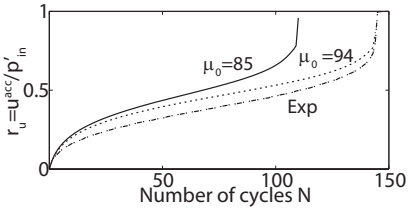

(b) test settings: $p'_{in} = 200\ kPa$, $e_{in} = 0.842$, $\varsigma = 0.2$, best fit $\mu_0 = 94$

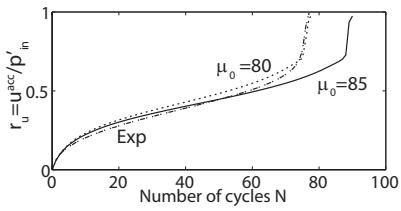

(c) test settings: $p'_{in} = 200\ kPa$, $e_{in} = 0.813$, $\varsigma = 0.25$, best fit $\mu_0 = 80$

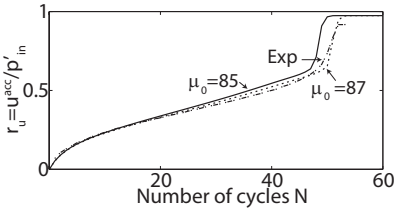

(d) test settings: $p'_{in} = 100\ kPa$, $e_{in} = 0.759$, $\varsigma = 0.3$, best fit $\mu_0 = 87$

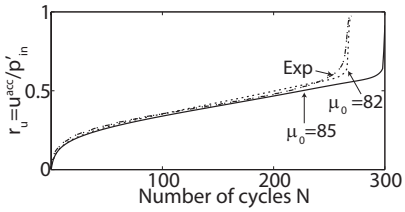

(e) test settings: $p'_{in} = 300\ kPa$, $e_{in} = 0.744$, $\varsigma = 0.3$, best fit $\mu_0 = 82$

Figure 8: Illustration of memory surface parameter μ_0 on pore water pressure pressure accumulation ratio under undrained conditions. Experimental results compared with new-model simulation results with average $\mu_0 = 85$ for all five sets and with simulation results with best-fit μ_0 value for each set.

REFERENCES

Andersen, K. (2015). Cyclic soil parameters for offshore foundation design. *Frontiers in Offshore Geotechnics III 5*.

Been, K. & M. G. Jefferies (1985). A state parameter for sands. *Géotechnique 35*(2), 99–112.

Corti, R., A. Diambra, D. M. Wood, D. E. Escribano, & D. F. Nash (2016). Memory surface hardening model for granular soils under repeated loading conditions. *Journal of Engineering Mechanics 142*(12), 04016102.

Corti, R., S. M. Gourvenec, M. F. Randolph, & A. Diambra (2017). Application of a memory surface model to predict whole-life settlements of a sliding foundation. *Computers and Geotechnics 88*, 152–163.

Dafalias, Y. F. & M. T. Manzari (2004). Simple plasticity sand model accounting for fabric change effects. *Journal of Engineering mechanics 130*(6), 622–634.

Escribano, D., D. Nash, & A. Diambra (2018). Local and global volumetric strain comparison in sand specimens subjected to drained cyclic and monotonic triaxial compression loading. *Geotechnical Testing Journal submitted for publication*.

Green, R., J. Mitchell, & C. Polito (2000). An energy-based excess pore pressure generation model for cohesionless soils. In *Proc.: Developments in Theoretical Geomechanics–The John Booker Memorial Symposium*, pp. 16–17. Sydney, New South Wales, Australia, Nov.

Houlsby, G., C. Abadie, W. Beuckelaers, & B. Byrne (2017). A model for nonlinear hysteretic and ratcheting behaviour. *International Journal of Solids and Structures 120*, 67–80.

Idriss, I. & R. Boulanger (2006). Semi-empirical procedures for evaluating liquefaction potential during earthquakes. *Soil Dynamics and Earthquake Engineering 26*(2), 115–130.

Lekarp, F. & A. Dawson (1998). Modelling permanent deformation behaviour of unbound granular materials. *Construction and building materials 12*(1), 9–18.

Li, X.-S. & Y. Wang (1998). Linear representation of steady-state line for sand. *Journal of geotechnical and geoenvironmental engineering 124*(12), 1215–1217.

Liu, H. Y., J. A. Abell, A. Diambra, & F. Pisanò (2018). A three-surface plasticity model capturing cyclic sand ratcheting. *Géotechnique submitted for publication*.

Pasten, C., H. Shin, & J. C. Santamarina (2013). Long-term foundation response to repetitive loading. *Journal of Geotechnical and Geoenvironmental Engineering 140*(4), 04013036.

Seed, H. B., P. P. Martin, & J. Lysmer (1975). *The generation and dissipation of pore water pressures during soil liquefaction*. College of Engineering, University of California.

Sweere, G. T. (1990). *Unbound granular bases for roads*. Ph. D. thesis.

Taiebat, M. & Y. F. Dafalias (2008). Sanisand: Simple anisotropic sand plasticity model. *International Journal for Numerical and Analytical Methods in Geomechanics 32*(8), 915–948.

Wichtmann, T. (2005). *Explicit accumulation model for non-cohesive soils under cyclic loading*. Ph. D. thesis, Inst. für Grundbau und Bodenmechanik Bochum University, Germany.

Wichtmann, T. & T. Triantafyllidis (2016). An experimental database for the development, calibration and verification of constitutive models for sand with focus to cyclic loading: part itests with monotonic loading and stress cycles. *Acta Geotechnica 11*(4), 739–761.